



UNIVERSITÀ DEGLI STUDI DI BERGAMO
DIPARTIMENTO DI INGEGNERIA DELL'INFORMAZIONE
E METODI MATEMATICI[°]

QUADERNI DEL DIPARTIMENTO

Department of Information Technology and Mathematical Methods

Working Paper

Series “*Mathematics and Statistics*”

n. 1/MS – 2012

***Impact of hemodynamics on lumen boundary displacements
in abdominal aortic aneurysms by means of dynamic
computed tomography and computational fluid dynamics***

by

M. Piccinelli, C. Vergara, L. Antiga, L. Forzenigo, P. Biondetti, M. Domanin

COMITATO DI REDAZIONE[§]

Series Information Technology (IT): Stefano Paraboschi
Series Mathematics and Statistics (MS): Luca Brandolini, Ilia Negri

[§] L'accesso alle *Series* è approvato dal Comitato di Redazione. I *Working Papers* della Collana dei Quaderni del Dipartimento di Ingegneria dell'Informazione e Metodi Matematici costituiscono un servizio atto a fornire la tempestiva divulgazione dei risultati dell'attività di ricerca, siano essi in forma provvisoria o definitiva.

IMPACT OF HEMODYNAMICS ON LUMEN BOUNDARY DISPLACEMENTS IN ABDOMINAL AORTIC ANEURYSMS BY MEANS OF DYNAMIC COMPUTED TOMOGRAPHY AND COMPUTATIONAL FLUID DYNAMICS

Marina Piccinelli¹ Christian Vergara² Luca Antiga³ Laura Forzenigo⁴

Pietro Biondetti⁴ Maurizio Domanin^{5,6}

1. Department of Mathematics and Computer Science, Emory University, Atlanta, Georgia, USA
2. Department of Engineering Information and Mathematical Methods, University of Bergamo, Italy
3. Biomedical Engineering Department, Mario Negri Institute, Bergamo, Italy
4. Operative Unit of Radiology, Fondazione I.R.C.C.S. Ca' Granda Ospedale Maggiore Policlinico, Milano, Italy
5. Department of Specialistic Surgery, University of Milan, Italy
6. Operative Unit of Vascular Surgery, Fondazione I.R.C.C.S. Ca' Granda Ospedale Maggiore Policlinico, Milano, Italy

Keywords: Time resolved computed tomography, abdominal aortic aneurysm, computational hemodynamics

ABSTRACT

Objective. The aim of the present work is to quantitatively assess the three dimensional (3D) distributions of the displacements experienced during the cardiac cycle by the luminal boundary of abdominal aortic aneurysm (AAA) in vivo and to correlate it with the local bulk hemodynamics.

Methods. Ten patients were acquired by means of time resolved computed tomography (4D-CT) and each patient-specific morphology of the abdominal aorta and aneurysmal sac was reconstructed for all available time frames. The AAA lumen boundary motion was successively tracked over the cardiac cycle and the lumen boundary displacement (LBD) computed for each time frame to a reference position selected at the mid-diastolic phase. The intra-aneurysm hemodynamic quantities, such as wall shear stress (WSS), were evaluated with a computational fluid dynamics (CFD) simulation performed on the reference geometry of each patient. The co-localization of LBD and WSS distributions was evaluated by means of Pearson correlation coefficient.

Results. A clear anisotropic distribution of LBD was evidenced in both space and time. AAA lumen boundary exhibited a combination of inward- and outward-directed motions throughout the cardiac cycle and specifically at time frames close to the systolic peak. For almost all the analyzed cases a co-localization between largest outward LBD and high WSS, taken as a surrogate of flow impingement, was demonstrated supporting our hypothesis of a mechanistic relationship between anisotropic displacement and hemodynamic forces related to the impingement of the blood on the lumen boundary.

Conclusions. The assessment of AAA lumen boundary anisotropic displacements may represent a promising direction for patient risk stratification and investigation of AAA progression. Four dimensional CT and patient-specific CFD may become valuable tools in research and clinical environments for patient management and pre-surgical evaluation.

INTRODUCTION

Abdominal aortic aneurysm (AAA) is a degenerative disease of the last segment of the aorta, representing 83% of all non-cerebral aneurysms diagnosed in the United States^{1,2}; if not treated an AAA may rupture, a severe clinical event associated with high rate of mortality and morbidity.

The pathogenesis of AAA is extremely complex and not completely understood³⁻⁵; in fact, aneurysm formation likely results from the interaction of multiple factors, such as smoking, hypertension and inflammation processes. In addition, local hemodynamic features, i.e. presence of reverse flow, pressure wave propagation and reflection and wall shear stress (WSS), have been acknowledged to play a leading role in AAA development and clinical outcome^{4,6-9}.

Since long researchers have struggled in the attempt to identify and elucidate the mechanisms leading to aneurysm initiation, progression and wall failure¹⁰. Despite many progresses, the majority of criteria proposed for risk stratification and decision making still rely on empirical measurements rather than on the analysis of biomechanical properties¹¹; among these, maximum AAA diameter¹², currently the prevalent index for the evaluation of risk of rupture, AAA expansion rate¹³, wall stiffness¹⁴, intraluminal thrombus thickness¹⁵ and AAA wall peak stress^{16,17}.

In this quest for elements that could contribute to the evolution of AAA towards its rupture, a rather overlooked phenomenon is the cyclical displacements experienced by vessel wall during the cardiac cycle. Indeed, recent works have underlined the anisotropic nature of these displacements at the level of AAA; uneven aortic motions were observed at the infrarenal level¹⁸ and significant aneurysm neck pulsatility was reported^{19,20}. Different concomitant causes could contribute to the occurrence of anisotropic displacements: complex AAA shape subjected to hydrostatic pressure changes, heterogeneity of mechanical properties of vessel

wall and intraluminal thrombus, outer anatomical constraints. Another compelling hypothesis is that they may be the result of the action of the intra-aortic bulk hemodynamics, impinging on the lumen surface, which is in turn associated to the altered anatomy of the abdominal aorta including the AAA.

Thanks to advances in both biomedical imaging and computational fluid dynamic (CFD) this issue can be directly address: in vivo AAA displacements can in fact be acquired noninvasively at different instants of the cardiac cycle with dynamic-four dimensional computed tomography (4D-CT), while intra-aortic hemodynamics (velocity and WSS distributions) can be computed by means of CFD on the same patient-specific geometry²¹.

The aim of this work is to quantitatively assess the three-dimensional (3D) distributions of the displacements experienced by AAA luminal boundary over the cardiac cycle as reconstructed from 4D-CT acquisitions, in relation to the hemodynamic variables obtained by CFD simulations. The availability of a mechanistic relationship between anisotropic displacements and bulk hemodynamics may shed new light on the role of hemodynamics in AAA progression studies and may influence the design of new rupture risk indices in the future, with direct implications on planning for surveillance and surgical intervention.

MATERIALS AND METHODS

Patient recruitment

Ten patients who underwent 4D-CT as preoperative evaluation of an AAA between July 2007 and December 2008 were selected at the Operative Unit of Vascular Surgery of the Ca' Grande Ospedale Maggiore Policlinico in Milan, Italy. All the patients were initially considered for EVAR due to hostile abdomen, high risk conditions, advanced age or patient choice. For all them, ethical review board approval and informed consent were obtained.

Detailed imaging data, physiological parameters and outcome data were collected prospectively.

Image acquisition: scanner and protocol

The acquisitions were performed with a Somatom Definition Double Source CT (Siemens, Erlanger, Germany), before and after contrast media administration with retrospectively electrocardiographic (ECG) gated spiral acquisition. Non-ionic contrast media (Iomeron, Bracco, Milan, Italy) was used with a concentration of 400 mg/I mg, 1.5 cc pro kg and an injection speed of 3 cc/s. The temporal resolution was 85 ms and the total effective dose according with the applied protocol was 34 mSv per acquisition and per patient. Ten ECG gated series of axial images were reconstructed at every 10% of the R-R interval from the aortic arch to the common femoral arteries, allowing the retrieval of dynamic imaging of the aorta during a complete systolic-diastolic cycle.

3D model reconstruction

All image processing operations, from 3D reconstruction to post processing, were performed by means of the Vascular Modeling Toolkit, VMTK²². For each dataset and for all the ten time frames the 3D surface model of the lumen surface of the aorta from the thoracic segment to the first tract of the common iliac arteries was reconstructed using a gradient-driven level set technique²³. The main side branches (celiac trunk, superior mesenteric artery, right and left renal arteries) were also included in the model. The 7th time frame corresponding to the mid-diastolic phase was selected as the reference one over the cardiac cycle for all subsequent analysis. For each subject, ten 3D triangulated surface models were then available to describe the location of the lumen boundary throughout the cardiac cycle.

Vascular geometric characterization

For each reference time frame a series of operations were performed to quantitatively characterize the geometry of the vascular segment at hand and to automatically identify the portion of the network hosting the AAA, namely the segment comprised between the origin of the renal arteries and the common iliac bifurcations²⁴, Figure 1a,b. Additionally, an automated separation of the lumen surface of the AAA in posterior and anterior sectors was performed by means of the bifurcation reference system²⁴ computed at the iliac bifurcation, Figure 1c. To this end, the bifurcation plane normal vector was computed and parallel transported along the centerline, an operation that allows a vector system to follow centerline curvature without introducing additional torsion²⁴. The line delineating the separation between anterior and posterior areas was hence identified on the AAA 3D surface, Figure 1d.

Lumen boundary motion tracking

To quantitatively evaluate the movement of the AAA lumen surface throughout the cardiac cycle, at each time frame the displacement of each point of the current 3D surface with respect to the 7th one was computed. Reference and current surfaces were first rigidly registered by means of the ICP algorithm²⁵ to disregard pure rigid motion. Successively, for each point on the current surface, the closest triangle on the reference surface was identified and the point displacement calculated as its Euclidean distance to the triangle. Finally, nine maps of displacements, hereafter indicated as *lumen boundary displacements* (LBD), were available for each patient. Positive (negative) values of displacement indicate an outward (inward) motion of the lumen boundary with respect to the mid-diastolic location (Fig. 2).

Numerical simulations

Once the geometry of the specific patient was reconstructed at the reference time frame, the surface model was turned into a volumetric mesh of linear tetrahedra (in the range 1.1-2.2

millions of elements) in view of unsteady CFD simulations performed using the finite element code LifeV²⁶. Blood was considered as a Newtonian, homogeneous and incompressible fluid, so that the Navier-Stokes equations were used for its mathematical description²¹. Blood viscosity was set equal to 0.035 Poise, density equal to $1.0 \text{ (g/cm}^3\text{)}^{21}$, and time step equal to 0.02s. Given the small magnitude of the observed displacements and the fact that flow impingement patterns are not expected to critically depend on perturbations of the boundary, rigid walls were adopted. At the inlet, the physiological flow rate $Q(t)$, chosen as representative of the physiological inflow (Fig. 3), was prescribed through a Lagrange multipliers approach^{23,27}. For each of the mesenteric and renal branches, we prescribed a flow rate equal to $Q(t)/20$ (with the assumption of flat profile), so that $4/5 Q(t)$ is the flow rate ultimately entering the AAA. At the two iliac outlets a zero-stress condition was prescribed, since the region of interest was far from them. No turbulence models were adopted, since transitional flow is supposed to be absent in the abdominal aorta²⁸. In order to allow a comparison between displacement maps and hemodynamics features, WSS (used as surrogate of flow impingement) maps were computed at the ten instants over the cycle.

Relationship between lumen boundary displacements and wall shear stress

To compare vector fields defined on the AAA surface, namely LBD and WSS, computational techniques to patch and flatten 3D surfaces were applied²⁹. In order to focus on the behavior of the lumen boundary in correspondence of the aneurysm, the beginning of the most upstream location of the aneurysmatic dilatation was identified by monitoring wall thickening, presence of thrombus or enlargement of aortic diameter. Firstly, contiguous rectangular regions were automatically defined on the 3D model and the quantities of interest averaged over the new domains. Secondly, the surface was “opened” at the line separating the anterior-posterior sectors (Figure 1d) and flattened on a parametric rectangular space

(Figure 1e). The flattened maps were obtained for all patient at each time frame, so that WSS and LBD were compared over these specific areas. In addition, a smoothing operation was performed on the rectangular maps by means of a Gaussian filter to remove spurious high frequencies in LBD and WSS, while retaining their global features.

Finally, Pearson's correlation index³⁰ between the two rectangular maps was calculated for each time frame and for each patient to quantify the co-localization of LBD and WSS.

RESULTS

Data of the population

The median age of the population was 72 years. Eight patients were male (80%) and 2 female (20%). The median height was 173 ± 9 cm, body weight 82.5 ± 15.41 kg, body mass index 27.56 ± 4.5 . Six patients had a history of smoking (60%), 6 suffered of hypertension (60%), 1 was diabetic (10%), 2 suffered of peripheral arterial disease (20%) and 2 had a miocardial infarction or aorto-coronary bypass graft surgery (20%).

Aneurysms were classified as small in 4 cases (40%) and medium in 6 (60%). The mean proximal neck diameter was 23.26 ± 4.00 mm (range 18.00-29.67) and length 4.12 ± 1.38 cm (range 2.5-6.63). The mean maximum aortic diameter was $50.53 \text{ cm} \pm 7.57$ (range 39.37-64.09), while the mean length of AAA $8.46 \text{ cm} \pm 3.49$ (range 5.1-16.0). Laminar thrombus in the aneurismal sac was not observed in 2 cases (20%), while it was largely present in 8 (80%). It was concentric in 6 cases (60%) and eccentric in 2 (20%).

Relation between lumen surface displacement and fluid dynamics

For each patient the 3D surfaces for all time frames were successfully reconstructed, the AAA portion isolated and the line separating the anterior/posterior sectors identified. The nine LBD and WSS maps were computed and their flattened versions obtained.

We observed that for all the analyzed cases the largest displacements occurred close to the systolic peak (3rd, 4th, 5th frame), while they globally faded away in the mid and late diastolic phases. Figure 4 depicts the LBD maps of the first patient for all the time frames, while Figures 5-7 report for the remaining cases only the maps for frames close to the systolic peak.

The qualitative analysis of LBD clearly highlighted the anisotropic distributions of the AAA lumen boundary displacements both space and time for all the analyzed cases: the portions of the AAA lumen boundary experiencing outward and inward motion were concentrated in different parts of the AAA surface and abruptly separated from each other. The outward motion was preferentially observed in the anterior sectors of the AAA lumen boundary.

The percentages of AAA surface area moving in the outward or inward direction with respect to the reference time frame were evaluated at all frames. A spike in the percentage of outer directed lumen boundary area was evidenced around the systolic peak with an average value of $67 \pm 12\%$ of the total AAA lumen boundary area (range between 25 - 82%); it decreased to $43 \pm 11\%$ (range 19 - 63%) during the late diastolic phase. The average percentage of AAA boundary lumen boundary moving in the inward direction was assessed at $35 \pm 15\%$ close to the systolic peak (range 18 - 84%) and increased during the diastolic phase to $57 \pm 12\%$ (range 36 - 81%). Notably, in all the analyzed cases and throughout the first half of the cardiac cycle the AAA lumen boundary exhibited a somewhat surprising combination of inward and outward motions, where the latter were however prevalent. This trend vanished for most cases in the second part of the cardiac cycle.

The analysis of the displacement values was then separately performed for areas undergoing outward and inward motion. For all the patients the largest displacements occurred at time frames close to the systolic peak in both inward and outward directions (Table 1). In only one case (patient 10) the displacement remained always below the in-plane image spacing (0.48 x 0.48 mm). In absolute terms, the outward displacement exceeded the inward one for all the analyzed cases except one (patient 6). When the 3rd, 4th and 5th frames were considered, the maximum outward LBD ranged between 0.55 and 1.40 mm (mean 0.75 ± 0.29 mm), and the maximum inward LBD ranged between 0.35 and 1.87 mm (mean 0.59 ± 0.35 mm). In all cases, both inward and outward displacement values at the systolic peak decidedly decreased during the mid and late diastolic phases, often below the image resolution.

WSS (Fig 4-7) exhibited similar distribution patterns: during the systolic phase areas of intense stresses alternated over the AAA lumen boundary with zones of rather mild friction, though we observed a strong dependence on the specific shape of the AAA sac at hand.

The comparison of LBD and WSS allows a qualitative assessment of the correlation, in time and space, between the two distributions, directly linking the AAA lumen boundary motion to the hemodynamic forces. The co-localization of outward motion and high WSS was clear at the systolic peak in half of the analyzed cases, particularly cases 1, 3, 4, 5, 9. For the other cases this relation was less clear, even though the maximum LBD and WSS still occurred at the systolic phase.

A quantitative analysis of the co-localization of LBD and WSS was performed computing the Pearson correlation coefficient between the maps values. Table 2 reports the index for each case at each frame. A relative increase in the correlation index is visible close to the systolic peak for all the cases except patient 6 (Fig. 6). The increase is particularly evident for cases 1,

3, 4, 5, 8, 9, while it is less abrupt for patients 2, 7, 10. Ultimately, in 4 cases there is at least one time frame with correlation index > 0.73 .

For a better representation of the flow patterns inside the AAA, the velocity field are shown in Figure 8 at the systolic peak for each case, together with the WSS map at the impingement area. These 3D representations can provide a more comprehensive picture of the complexity of flow features: the direction of the blood jet coming from the aorta, its impact on the lumen boundary and their relation to LBD, also reported. For some of the cases with a relatively high correlation coefficient these figures further evidence the correspondence between the zone impacted by the blood and the outward LBD (cases 1, 3, 4, 8, 9). Coherently, in case 6, which exhibited a low correlation coefficient, the blood jet was aligned along the axial direction of the vessel and no pattern was detectable in the LBD map. Figure 8 also highlighted the strong influence of the aorta geometry in determining the direction of impact.

DISCUSSION

The mechanisms that lead to AAA development, progression and rupture are still unclear and most probably implicate a number of factors from family history, vascular wall biology and hemodynamic features^{4,6,32}. Several indices have been proposed for the classification of aneurysms depending on their likelihood to rupture, but most of them fail to account for the phenomena occurring at the vascular wall and for the specificity of the patient^{10,11,13-16}.

The focus of this work was the assessment and quantification of anisotropic displacements experienced by AAA lumen boundary throughout the cardiac cycle. 4D-CT acquisitions have been employed to evaluate aneurysmal lumen boundary motion, while specific hemodynamic features have been investigated as a potential explanation for such displacements by means of CFD simulations in the specific patient anatomy.

The importance of wall motion due to the pulsatile nature of the blood flow has been considered in some recent work¹⁸⁻²⁰ and, consistently, emphasis has been placed on the necessity of performing dynamic imaging of AAA instead of traditional static acquisition in order to account for these phenomena³¹. In these works¹⁸⁻²⁰ the authors measured anisotropic wall motions at several locations along the infrarenal segment but mostly on 2D images. Instead, in the present study we focused on obtaining a complete 3D description of the displacements of the AAA and its parent vasculature throughout the cardiac cycle by means of 4D-CT imaging. To the authors' knowledge this is the first attempt to use this methodology to study lumen boundary displacement quantitatively in vivo.

By means of this technique, we assessed the presence of anisotropic displacements of the AAA lumen boundary. In all analyzed cases but one, at the systolic peak considerable portions of the lumen boundary, usually of the anterior sector, were found to move outward with respect to the reference position, while others to move inward. Such strong anisotropy progressively vanished in the remaining parts of the cycle. The presence of strongly heterogeneous in space and time LBD may potentially affect the biomechanics of AAA, in terms of distribution and magnitude of strains and stresses, influence biological processes such as wall remodeling, and ultimately determine the evolution of AAA towards rupture.

The concurrent presence of outward and inward displacements at systole is an interesting observation by itself. In the classical view, vascular structures are supposed to expand and relax concentrically respectively at systole and diastole, due to the effect of hydrostatic pressure. Our results demonstrated that this is not necessarily the case, and that AAA displacement is probably caused, or at least contributed by, hemodynamic forces related to the impingement of the blood on the lumen boundary. Indeed, hydrostatic pressure alone, even in combination with complex geometry, would hardly be sufficient to explain this

phenomenon: during systole the impingement of the jet on the AAA lumen boundary determines outward motion of the impacted area, while other regions not subjected to such dynamic pressure “accommodated” the resulting displacement with opposite inward motion. During diastole, the less energetic flow reorganizes within the AAA volume, no specific trend or correlation is noticeable and the displacement magnitude significantly decreases.

The co-localization between large LBD and high WSS was not equally evident in all the cases. This is not surprising, since a high correlation is expected only for those cases where flow impingement occurs on the sac due to the specific morphology of the abdominal aorta, whilst it is expected to be absent when the blood flow is aligned with the vessel wall and the impingement occurs directly at the iliac bifurcation. This is strongly patient dependent, since it is the proximal aorta geometry and the sac morphology that eventually determine the presence of an impingement region and, according to our hypothesis, of an AAA lumen boundary anisotropic motion (Fig. 8). This makes the assessment of anisotropic boundary displacements and of high viscous forces on the sac a potentially informative tool to evaluate the status of a specific AAA and, at the same time, it makes the specific morphology of the abdominal aorta a potential predictor of the actual biomechanical environment.

The present study was not aimed at determining a cause-effect relationship between displacements and rupture, but at documenting the existence of cyclic anisotropic displacements and at suggesting a direct physical explanation for their occurrence. To this end, some limitations of this study should be mentioned. For the CFD simulations, a rigid wall hypothesis was adopted, instead of performing a fluid-structure interaction analysis. This choice was made since we were interested in localizing the regions of the sac surface where the WSS was higher, not in determining its precise value. For this reason, we believe that the rigid wall assumption is acceptable for our aims, and it simplifies the analysis remarkably.

The presence of the intraluminal thrombus was not considered in this work. While acknowledging its importance for a proper description of the mechanical environment, the goal of the present study was to verify the impact of the bulk flow on the lumen boundary, i.e. on the interface in direct contact with the blood.

CONCLUSIONS

The assessment of AAA sac cyclical displacements and their anisotropy may represent a promising direction for patient risk stratification and prediction of AAA evolution. As new means of investigation such 4D-CT and patient-specific CFD become widely available, such evaluations may play a role in research and clinical environments for patient management, pre-surgical evaluation and follow-up planning.

ACKNOWLEDGMENTS

The authors would like to thank Barbara Barberis and Alessandro Duci.

FUNDING SOURCES

This study has been performed with a partial funding of the Fondazione Cà Granda Ospedale Policlinico, Milan, Italy. C. Vergara has been partially supported by the ERC Advanced Grant N.227058 MATHCARD.

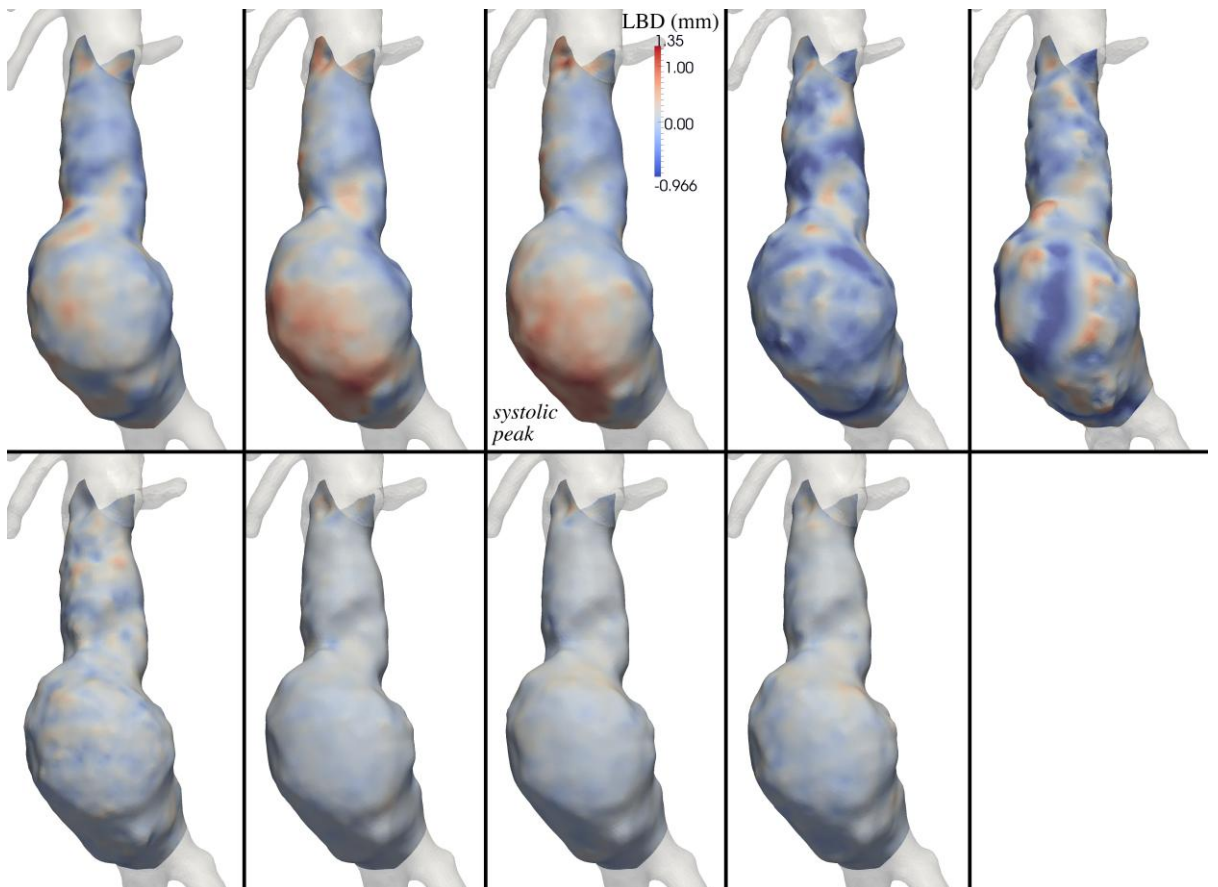
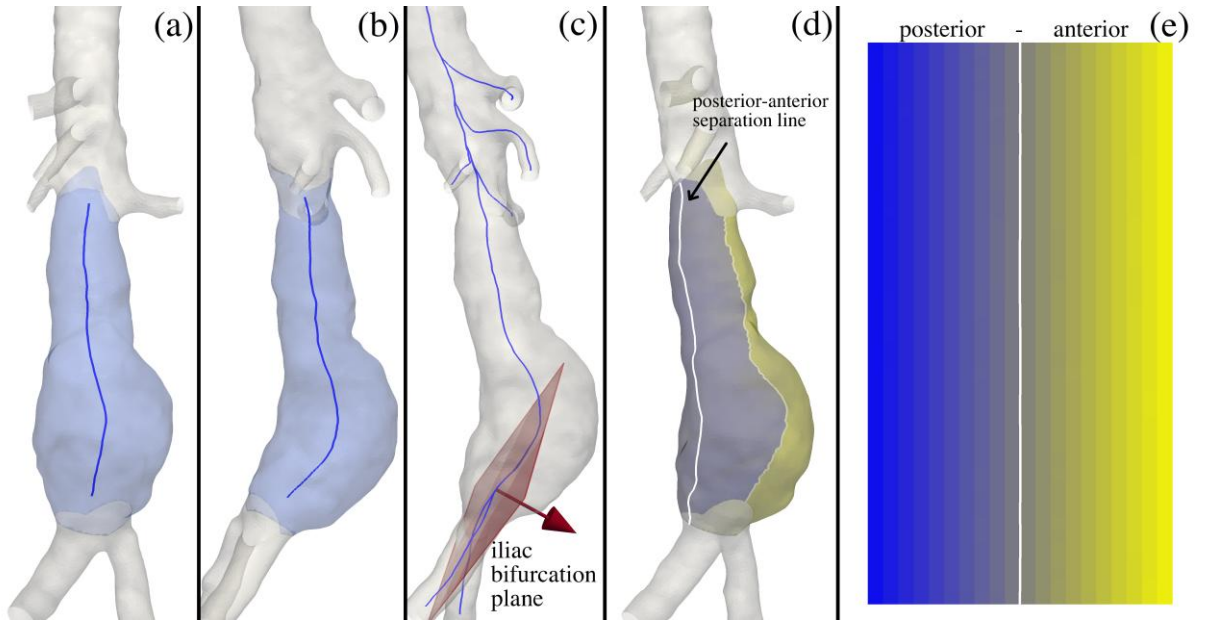
REFERENCES

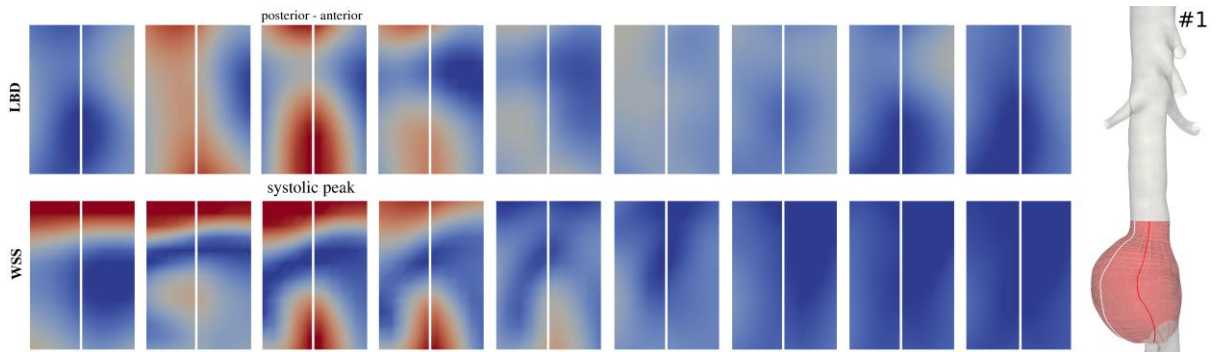
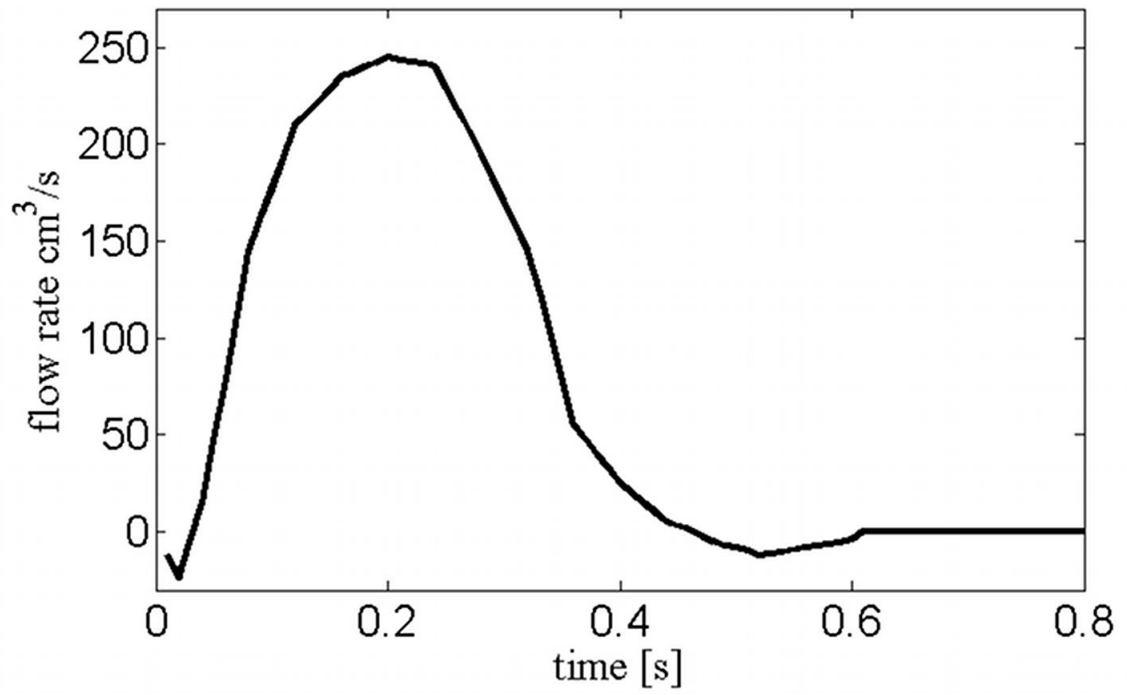
1. Lawrence PF, Gazak C, Bhirangi L, Jones B, Bhirangi K, Oderich G, Treiman G. The epidemiology of surgically repaired aneurysms in the United States. *J Vasc Surg*, 1999; 30:632-40.
2. Gillum RF. Epidemiology of aortic aneurysm in the United States. *J Clin Epidemiol*, 1995; 48:1289-98.
3. Grange JJ, Davis V, Baxter BT. Pathogenesis of aortic abdominal aneurysms: an update and look toward the future. *Cardiovasc Res*, 1997; 5(3): 256-65.
4. Dalman RL, Tedesco MM, Myers J, Taylor CA. Mechanisms, stratification and treatment. *Ann N Y Acad Sci*, 2006; 1085: 92-109.
5. Michel JB, Martin-Ventura JL, Egido J, Sakalihasan N, Treska V, Lindholt J, Allaire E, Thorsteinsdottir U, Cockerill G, Swedenborg J, FAD EU consortium. Novel aspects of the pathogenesis of aneurysms of the abdominal aorta in humans. *Cardiovasc Res*, 2011; 90(1): 18-27.
6. Dua MM, Dalman RL. Hemodynamics influences on abdominal aortic aneurysm disease: application of biomechanics to aneurysm pathophysiology. *Vascul Pharmacol*, 2010; 53(1-2): 11-21.
7. Nixon AM, Gunel M, Sumpio BE. The critical role of hemodynamics in the development of cerebral vascular disease. *J Neurosurg*, 2010; 112(6): 1240-53.
8. Hoshina K, Sho E, Sho M, Nakahashi TK, Dalman RL. Wall shear stress and strain modulate experimental aneurysm cellularity. *J Vasc Surg*, 2003; 37: 1067-74.

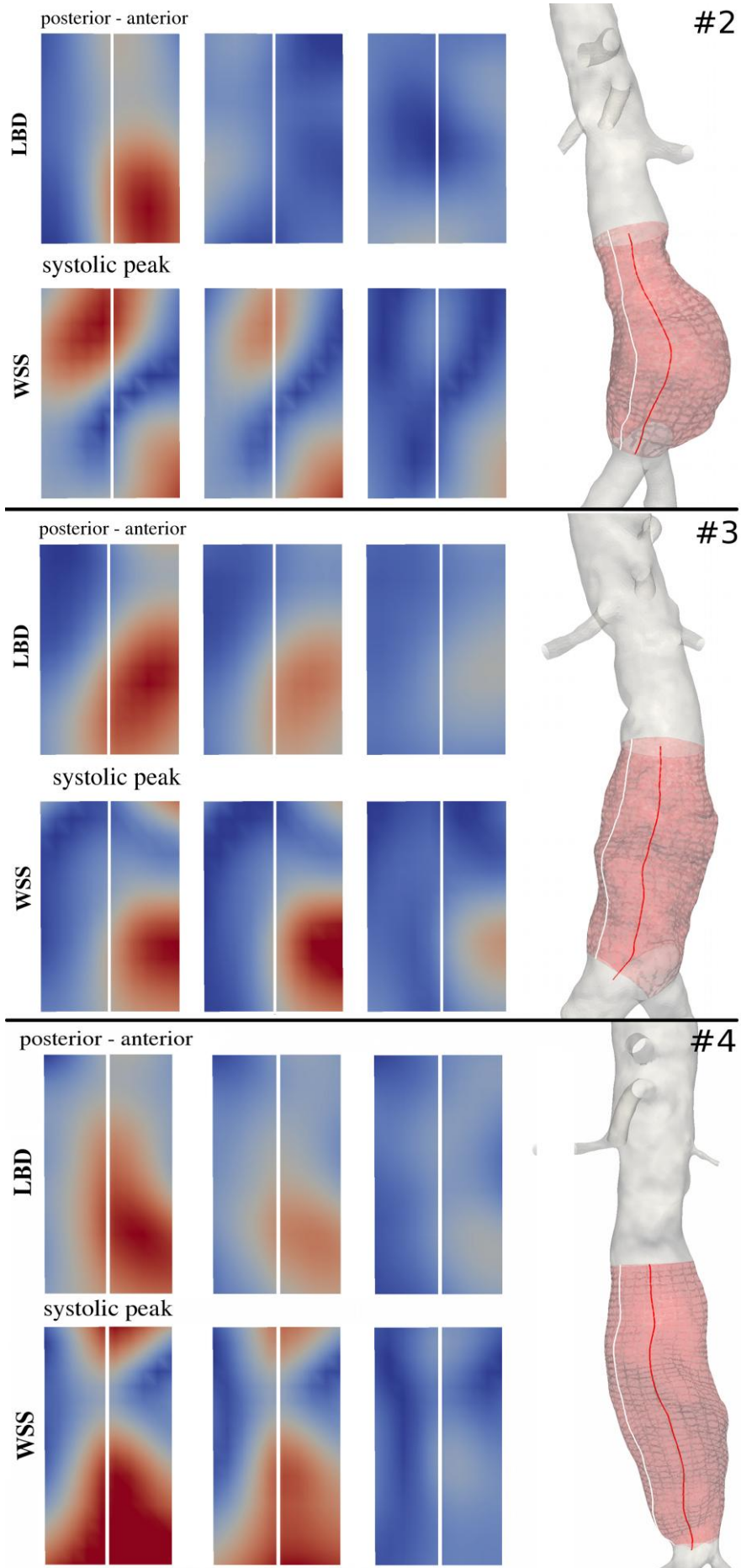
9. Bousset L, Rayz V, McCulloch C, Martin A, Acevedo-Bolton G, Lawton M, et al. Aneurysm growth occurs at region of low Wall Shear Stress. Patient-specific correlation of hemodynamics and growth in a longitudinal study. *Stroke*, 2008; 39: 2997-3002.
10. Vorp DA. Biomechanics of abdominal aortic aneurysm. *J. Biomech.* 2007; 40(9): 1887–902.
11. Hua J, Mower WR. Simple geometric characteristics fail to reliably predict abdominal aortic aneurysm wall stresses. *J Vasc Surg*, 2001; 34:308-15.
12. Greenhalgh R, Brown LC, Kwong GP, Powell JT, Thompson SG. Comparison of endovascular aneurysm repair with open repair in patients with abdominal aortic aneurysm (EVAR trial 1), 30-day operative mortality results: randomised controlled trial. *Lancet* 2004; 364 (9437):843–8.
13. Hirose y, Takamiya M. Growth curve of ruptured aortic aneurysm. *J Cardiovasc Surg* 1998; 39: 9-13.
14. Fillinger MF, Marra SP, Raghavan ML, Kennedy FE. Prediction of rupture risk in abdominal aortic aneurysm during observation: wall stress versus diameter. *J Vasc Surg.* 2003; 37:724 –732.
15. Speelman L, Schurink GWH, Bosboom EMH, Buth J, Breeuwer M, van de Vosse FN, Jacobs MH. The mechanical role of thrombus on the growth rate of an abdominal aortic aneurysm. *J Vasc Surg*, 2010; 51: 19-26.

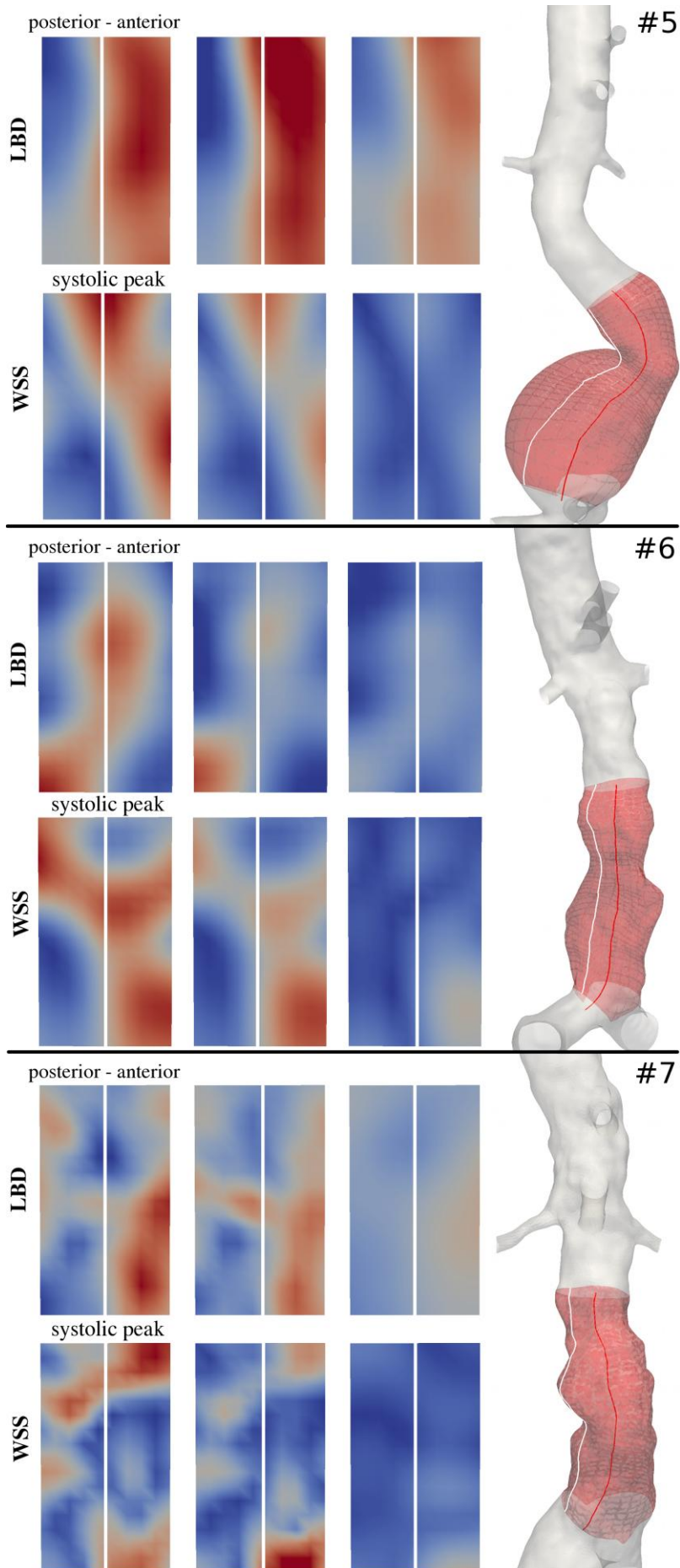
16. Raghavan ML, Vorp DA, Federle MP, Makaroun MS, Webster MW. Wall stress distribution on three-dimensionally reconstructed models of human abdominal aortic aneurysm. *J Vasc Surg*, 2000; 31(7): 760-9.
17. McGloughlin TM, Doyle BJ. New approaches to abdominal aortic aneurysm rupture risk assessment. Engineering insights with clinical gain. *Arterioscler Thromb Vasc Biol*, 2010; 30: 1687-94.
18. Arko FR, Murphy EH, Davis III CM, Johnson ED, Smith ST, Zarins CK. Dynamic geometry and wall thickness of the aortic neck of abdominal aortic aneurysms with intravascular ultrasonography. *J Vasc Surg*, 2007; 46: 891-7.
19. Van Herwaarden JA, Bartels LW, Muhs BE, Vincken KL, Lindeboom MY, Teutelink A, Moll FL, Verhagen HJ. Dynamic magnetic resonance angiography of the aneurysm neck: conformational changes during the cardiac cycle with possible consequences for endograft and future design. *J Vasc Surg*, 2006; 44:22-8.
20. Vos AWF, Wisselink W, Marcus JT, Vahl AC, Manoliu RA, Rauwerda JA. Cine MRI assessment of aortic aneurysm dynamics before and after endovascular repair. *J endovasc Ther*, 2003; 10: 433-39.
21. Formaggia L, Quarteroni A, Veneziani A. Cardiovascular Mathematics – Modeling and simulation of the circulatory system. Springer; 2009.
22. Antiga L, Steinman DA. The Vascular Modeling Toolkit. Available at <http://www.vmtk.org>. Accessed December 2011.

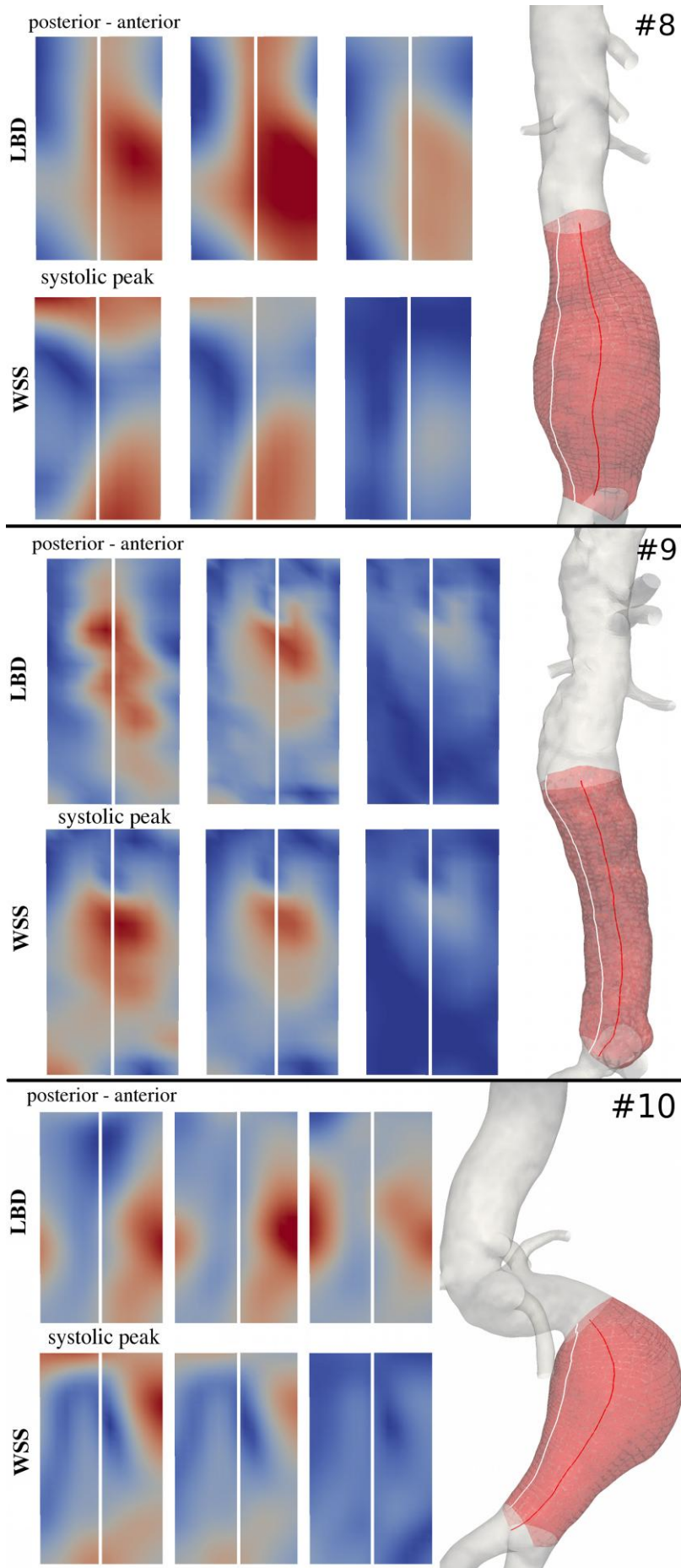
23. Antiga L, Piccinelli M, Botti L, Ene-Iordache B, Remuzzi A, Steinman DA. An image-based modeling framework for patient-specific hemodynamics. *Med Biol Eng Comput*, 2008; 46:1097-112.
24. Piccinelli M, Veneziani A, Steinman DA, Remuzzi A, Antiga L. A framework for geometric analysis of vascular structures: applications to cerebral aneurysms. *IEEE Trans Med Imag*, 2009; 28:1141-55.
25. Besl PJ, McKay ND. A method for registration of 3D shapes. *IEEE Trans Pattern Anal Machine Intellig*, 1992; 14:239-56.
26. LIFEV software. Available at <http://www.lifev.org>. Accessed December 2011.
27. Veneziani A, Vergara C. Flow rate defective Boundary Conditions in Haemodynamics Simulations. *Int. Journ. Num. Meth. Fluids*, 2005;47:803-16.
28. Nichols WW, O'Rourke MF. McDonald's blood flow in arteries: Theoretical, experimental and clinical principles. Edward Arnold, 1998.
29. Antiga L, Steinman DA. Robust and objective decomposition and mapping of bifurcating vessels. *IEEE Trans Med Imag*, 2004; 23:704-13.
30. R Development Core Team. R: A language and environment for statistical computing. Vienna, Austria. <http://www.R-project.org>. Accessed December 2011.
31. Laskowski I, Verhagen HJM, Gagne PJ, Moll FL, Muhs BE. Current state of dynamic imaging in endovascular aortic aneurysm repair. *J Endovasc Ther*, 2007; 14: 807-12.
32. Malek AM, Alper SL, Izumo S. Hemodynamic shear stress and its role in atherosclerosis. *JAMA*, 1999; 282: 2035-42.

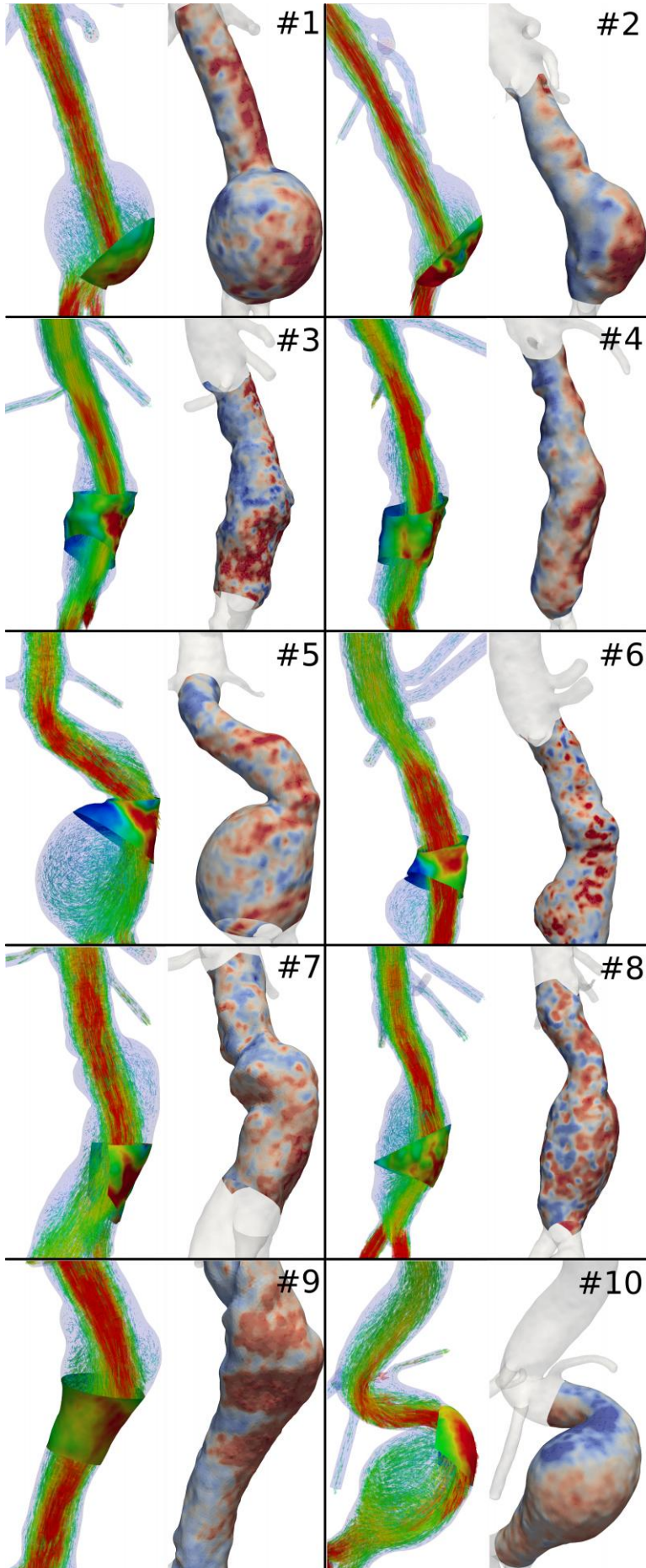












Figures captions

Figure 1. 3D model of AAA and close vasculature. a-b) AAA sac (opaque blue) and centerline; two different orientations of the model are shown to highlight the 3D nature of the aneurysmal sac; c) definition of the bifurcation plane at the iliac bifurcation; by means of the plane normal (red) the separation of the AAA surface model in an anterior and posterior sectors can be performed; d) each point on the AAA surface is associated with a circumferential angle, here plotted, from 0 to 3.14 radians (anterior sector) and from 0 to -3.14 radians (posterior sector); e) flattening procedure of the AAA 3D surface into a rectangular domain; the angular metric is plotted and the line separating in the anterior and posterior sectors indicated.

Figure 2. The nine LBD maps for all the time frames with respect to the reference position are shown for patient 2. The third corresponds to the systolic peak. Red (blue) color represents outward (inward) AAA lumen boundary motion with respect to the reference position

Figure 3. Flow rate prescribed at the inlet of the computational domain. This waveform has been chosen as representative of the physiological one.

Figure 4. Flattened and smoothed maps of LBD (top) and WSS (bottom) for patient 01 at all frames. The reconstructed 3D model is also depicted at the seventh time frame; AAA sac (red surface) and its centerline (red line) are indicated.

Figure 5. Flattened and smoothed maps of LBD (top) and WSS (bottom) for patients 02, 03, 04 at 3rd (systolic peak), 4th and 5th time frames; red (blue) color represents outward (inward) AAA lumen boundary motion with respect to the reference position and high (low) WSS. The reconstructed 3D model is also depicted at the seventh time frame; AAA sac (red surface) and its centerline (red line) are indicated.

Figure 6. Flattened and smoothed maps of LBD (top) and WSS (bottom) for patients 05, 06, 07 at 3rd (systolic peak), 4th and 5th time frames; red (blue) color represents outward (inward) AAA lumen boundary motion with respect to the reference position and high (low) WSS. The

reconstructed 3D model is also depicted at the seventh time frame; AAA sac (red surface) and its centerline (red line) are indicated.

Figure 7. Flattened and smoothed maps of LBD (top) and WSS (bottom) for patients 08, 09, 10 at 3rd (systolic peak), 4th and 5th time frames; red (blue) color represents outward (inward) AAA lumen boundary motion with respect to the reference position and high (low) WSS. The reconstructed 3D model is also depicted at the seventh time frame; AAA sac (red surface) and its centerline (red line) are indicated.

Figure 8. 3D models with velocity vectors identifying the different behavior of jet flow and the impingement area on the AAA lumen boundary (left) with LBD maps (right) at systolic peak.

Table 1. Measurements of outward and inward displacement per time frame. The instants around the systolic peak are highlighted.

patient	MAXIMUM - MINIMUM LBD								
	10%	20%	30%	40%	50%	60%	80%	90%	100%
<i>outward motion</i>									
01	0.35 - 0.09	0.88 - 0.18	0.85 - 0.22	0.76 - 0.14	0.50 - 0.10	0.51 - 0.09	0.41 - 0.08	0.44 - 0.09	0.38 - 0.07
02	1.00 - 0.22	1.35 - 0.41	1.40 - 0.43	1.21 - 0.22	1.37 - 0.28	0.53 - 0.1	0.40 - 0.05	0.4 - 0.05	0.47 - 0.07
03	0.42 - 0.06	0.56 - 0.09	0.71 - 0.11	0.66 - 0.07	0.48 - 0.05	0.40 - 0.04	0.29 - 0.04	0.34 - 0.03	0.39 - 0.05
04	0.60 - 0.13	0.88 - 0.25	1.05 - 0.26	0.85 - 0.17	0.53 - 0.13	0.53 - 0.11	0.42 - 0.09	0.4 - 0.07	0.46 - 0.1
05	0.39 - 0.05	0.47 - 0.07	0.55 - 0.10	0.55 - 0.11	0.5 - 0.08	0.31 - 0.05	0.27 - 0.04	0.36 - 0.05	0.47 - 0.06
06	0.50 - 0.07	0.67 - 0.09	0.73 - 0.11	0.70 - 0.10	0.76 - 0.09	0.96 - 0.08	0.58 - 0.07	0.67 - 0.07	0.62 - 0.07
07	0.56 - 0.06	0.63 - 0.10	0.57 - 0.10	0.56 - 0.08	0.43 - 0.07	0.42 - 0.06	0.51 - 0.05	0.49 - 0.05	0.60 - 0.05
08	0.57 - 0.10	1.07 - 0.21	1.05 - 0.24	1.32 - 0.29	0.88 - 0.19	0.94 - 0.18	0.92 - 0.15	0.76 - 0.13	0.76 - 0.12
09	0.47 - 0.05	0.76 - 0.13	0.72 - 0.17	0.77 - 0.12	0.72 - 0.06	0.6 - 0.04	0.36 - 0.03	0.35 - 0.04	0.41 - 0.05
10	0.21 - 0.04	0.38 - 0.07	0.33 - 0.07	0.49 - 0.07	0.39 - 0.06	0.34 - 0.03	0.20 - 0.03	0.24 - 0.03	0.23 - 0.03
<i>inward motion</i>									
01	0.51 - 0.12	0.48 - 0.10	0.56 - 0.11	0.71 - 0.12	0.65 - 0.10	0.49 - 0.07	0.46 - 0.09	0.59 - 0.12	0.52 - 0.12
02	1.12 - 0.27	1.10 - 0.28	0.97 - 0.27	1.39 - 0.40	1.87 - 0.40	0.53 - 0.10	0.40 - 0.05	0.43 - 0.06	0.40 - 0.08
03	0.45 - 0.05	0.28 - 0.04	0.36 - 0.03	0.49 - 0.03	0.41 - 0.03	0.46 - 0.04	0.40 - 0.04	0.50 - 0.05	0.55 - 0.06
04	0.60 - 0.12	0.42 - 0.10	0.53 - 0.09	0.42 - 0.08	0.37 - 0.08	0.41 - 0.08	0.48 - 0.10	0.66 - 0.12	0.81 - 0.16
05	0.31 - 0.06	0.33 - 0.06	0.41 - 0.07	0.44 - 0.07	0.36 - 0.05	0.30 - 0.04	0.29 - 0.05	0.29 - 0.06	0.29 - 0.07
06	0.55 - 0.07	0.45 - 0.05	0.58 - 0.06	0.68 - 0.06	0.53 - 0.06	0.48 - 0.06	0.72 - 0.06	0.53 - 0.07	0.49 - 0.08
07	0.41 - 0.05	0.69 - 0.07	0.55 - 0.07	0.40 - 0.06	0.40 - 0.05	0.43 - 0.05	0.32 - 0.05	0.32 - 0.05	0.41 - 0.05
08	0.76 - 0.16	0.79 - 0.17	0.84 - 0.17	0.92 - 0.22	0.77 - 0.15	0.76 - 0.14	0.75 - 0.15	0.81 - 0.17	0.80 - 0.17
09	0.57 - 0.05	0.34 - 0.05	0.45 - 0.07	0.57 - 0.05	0.35 - 0.03	0.20 - 0.02	0.52 - 0.03	0.56 - 0.04	0.53 - 0.06
10	0.13 - 0.02	0.22 - 0.04	0.24 - 0.04	0.23 - 0.03	0.32 - 0.02	0.19 - 0.02	0.13 - 0.02	0.18 - 0.03	0.21 - 0.03

10%, ... , 100% = percentage of cardiac cycle
30% = systolic peak

Table 2. Pearson correlation index between LBD and WSS maps at each time frame. The instants around the systolic peak are highlighted.

<i>patient</i>	Pearson Correlation Index (LBD - WSS)								
	10%	20%	30%	40%	50%	60%	80%	90%	100%
01	0.09	0.41	0.61	0.75	0.17	-0.11	-0.16	-0.31	-0.11
02	-0.84	-0.13	0.50	0.07	0.36	-0.42	0.37	0.74	0.85
03	0.40	0.79	0.89	0.89	0.76	0.51	-0.72	-0.43	-0.31
04	0.30	0.61	0.73	0.73	0.55	-0.24	-0.53	-0.43	-0.11
05	0.16	-0.21	0.43	0.55	0.35	-0.22	-0.12	-0.05	-0.21
06	-0.28	-0.001	0.06	-0.07	0.04	-0.06	-0.12	-0.10	-0.04
07	-0.02	0.09	0.14	0.29	0.46	0.46	0.02	0.07	-0.03
08	-0.01	-0.57	0.27	0.65	0.79	0.24	-0.49	-0.42	-0.14
09	-0.02	0.31	0.57	0.61	0.31	-0.11	0.04	0.02	0.24
10	-0.37	0.01	0.34	0.27	-0.04	0.28	0.33	0.53	0.41

10%, ... , 100% = percentage of cardiac cycle

30% = systolic peak